

## An Improved Three-Dimensional Simulation of the Diurnally Varying Street-Canyon Flow

Neda Yaghoobian · Jan Kleissl · Kyaw Tha Paw U

Received: 6 December 2013 / Accepted: 3 June 2014 / Published online: 8 July 2014  
© Springer Science+Business Media Dordrecht 2014

**Abstract** The impact of diurnal variations of the heat fluxes from building and ground surfaces on the fluid flow and air temperature distribution in street canyons is numerically investigated using the PARallelized Large-eddy Simulation Model (PALM). Simulations are performed for a 3 by 5 array of buildings with canyon aspect ratio of one for two clear summer days that differ in atmospheric instability. A detailed building energy model with a three-dimensional raster-type geometry—Temperature of Urban Facets Indoor-Outdoor Building Energy Simulator (TUF-IOBES)—provides urban surface heat fluxes as thermal boundary conditions for PALM. In vertical cross-sections at the centre of the spanwise canyon the mechanical forcing and the horizontal streamwise thermal forcing at roof level outweigh the thermal forces from the heated surfaces inside the canyon in defining the general flow pattern throughout the day. This results in a dominant canyon vortex with a persistent speed, centered at a constant height. Compared to neutral simulations, non-uniform heating of the urban canyon surfaces significantly modifies the pressure field and turbulence statistics in street canyons. Strong horizontal pressure gradients were detected in streamwise and spanwise canyons throughout the day, and which motivate larger turbulent velocity fluctuations in the horizontal directions rather than in the vertical direction. Canyon-averaged turbulent kinetic energy in all non-neutral simulations exhibits a diurnal cycle following the insolation on the ground in both spanwise and streamwise canyons, and it is larger when the canopy bottom surface is paved with darker materials and the ground surface temperature is higher as a result. Compared to uniformly distributed thermal forcing on urban surfaces, the present

---

N. Yaghoobian · J. Kleissl (✉)  
Department of Mechanical and Aerospace Engineering, University of California San Diego,  
La Jolla, CA, USA  
e-mail: jkleissl@ucsd.edu

*Present address:*

N. Yaghoobian  
Department of Mechanical Engineering, University of Maryland, College Park, MD, USA

K. T. Paw U  
Department of Land, Air, and Water Resources, University of California, Davis, Davis, CA, USA

analysis shows that realistic non-uniform thermal forcing can result in complex local airflow patterns, as evident, for example, from the location of the vortices in horizontal planes in the spanwise canyon. This study shows the importance of three-dimensional simulations with detailed thermal boundary conditions to explore the heat and mass transport in an urban area.

**Keywords** Diurnal Cycle · Heterogeneous thermal forcing · Large-eddy simulation · Urban canyon

## 1 Introduction

Urban microclimate that is affected by urban canyon geometry, weather conditions, anthropogenic heat fluxes, and physical, thermal and radiative properties of materials, directly affects the life of urban dwellers. Effects of microscale meteorological processes in urban canyons on energy use, human health and comfort have motivated many investigations over the past several decades (e.g. [Berg and Quinn 1978](#); [Rosenfeld et al. 1995](#); [Akbari and Rainer 2000](#); [Doulos et al. 2004](#); [Bouyer et al. 2011](#); [Wang et al. 2012](#)). Due to the complex flow patterns in the urban roughness layer, the lack of accurate information on thermal forcing from urban surfaces, and also experimental and numerical limitations for holistically studying the flow field and heat transport, typically only simplified abstractions of real urban canyons can be investigated. Several numerical (e.g. [Sini et al. 1996](#); [Kim and Baik 1999, 2001, 2010](#); [Xie et al. 2005, 2007](#); [Castillo et al. 2009](#); [Dimitrova et al. 2009](#); [Cheng et al. 2009](#); [Park et al. 2012, 2013](#); [Li et al. 2012](#); [Cai 2012](#); [Boppana et al. 2013](#); [Park and Baik 2013](#)) field measurement (e.g. [Nakamura and OkeTR, 1988](#); [Louka et al. 2002](#); [Eliasson et al. 2006](#); [Offerle et al. 2007](#); [Idczak et al. 2007](#); [Kitous et al. 2012](#)) and laboratory experimental (e.g. [Uehara et al. 2000](#); [Kovar-Panskus et al. 2002](#); [Allegrini et al. 2013](#)) studies investigated airflow, heat and mass transport in the urban roughness layer considering factors such as canyon aspect ratios, canyon/building configurations (e.g. variable building heights), orientation of the heated surfaces with respect to the wind direction, and ambient wind speed. In most numerical and laboratory experimental studies of the flow field and heat transport in street canyons, thermal forces were prescribed uniformly on canyon surfaces and did not vary with time. However thermal forces from urban street canyon surfaces under solar radiation are spatially and temporally variable according to the thermal and radiative properties of the construction materials (e.g. windows versus wall materials, or bright high-albedo surfaces versus dark low-albedo surfaces) and also seasonally- and diurnally-varying solar incidence angles. The latter also depends on the location and geometric characteristics of the built-up area (such as building block densities and street orientations).

A few studies investigated the impacts of heating in the urban canopy that were either time-dependent or contained sub-surface spatial heterogeneity. [Kwak et al. \(2011\)](#) incorporated urban surface and radiative processes into a computational fluid dynamic (CFD) model to investigate the *diurnal variation* of a two-dimensional (2-D) street canyon flow. However, thermal forces at each time were uniformly distributed over each canyon surface. [Solazzo and Britter \(2007\)](#) conducted CFD of a 2-D urban canyon in which the canyon's bounding facets were partially, but uniformly, heated (insolated), and assumed that the shaded fraction of the canyon was at the same temperature as the ambient flow. However, the mixing inside the canyon overcame the spatial heterogeneity and produced a spatially uniform air temperature distribution within the canyon. The lack of more realistic numerical investigations of the effects of heterogeneous heating on the airflow and pollutant dispersion within street canyons has been lamented by various investigators

(e.g. [Vardoulakis et al. 2003](#); [Xie et al. 2007](#); [Kwak et al. 2011](#); [Cai 2012](#)). The literature review shows that despite a long history of valuable urban microclimate studies, realistic dynamic and heterogeneous studies of heat transfer and flow in the urban canopy layer are still in preliminary stages.

The objective of this study is to apply the heat-flux distribution over each surface of a detailed 3-D building energy model as thermal boundary conditions into large-eddy simulation (LES) to provide a more comprehensive and realistic simulation of the diurnally-varying street-canyon airflow and temperature field. The building energy model, the LES, and their simulation set-up are described in Sect. 2. In Sect. 3, validation against wind-tunnel experimental data is performed. The results are presented and discussed in Sect. 4, and a summary and conclusions are given in Sect. 5.

## 2 Model Description and Simulation Set-Up

The PARallelized Large-eddy Simulation Model (PALM) developed at the Leibniz University of Hannover ([Raasch and Schröter 2001](#); [Letzel et al. 2008](#)) solves the filtered, incompressible Boussinesq equations, the first law of thermodynamics, the passive scalar equation, and the equation for subgrid-scale (SGS) turbulent kinetic energy (TKE). The SGS turbulent fluxes are parametrized using the 1.5-order [Deardorff \(1980\)](#) scheme for SGS TKE to calculate eddy viscosity. In PALM, momentum fluxes at the computational grid points adjacent to the solid surfaces are modelled based on Monin–Obukhov similarity with a stability correction as a function of local Richardson number. A detailed description of PALM can be found in [Letzel et al. \(2008\)](#).

Thermal fluxes from the solid surfaces in PALM are based on the Temperature of Urban Facets Indoor–Outdoor Building Energy Simulator (TUF-IOBES; [Yaghoobian and Kleissl 2012a](#)) fields. TUF-IOBES is a building-to-canopy model that simulates indoor and outdoor building surface temperatures and heat fluxes to estimate cooling/heating loads and energy use of buildings in a 3-D urban area. The indoor and outdoor energy balance processes are dynamically coupled taking into account weather conditions, indoor heat sources, building and urban material properties, composition of the building envelope (e.g. windows, insulation), and HVAC (heating, ventilation, and air conditioning) equipment. Further details of TUF-IOBES are described in [Yaghoobian and Kleissl \(2012a\)](#). Surfaces in the geometry of TUF-IOBES are subdivided into patches of identical size that represent walls, rooves, and streets (Fig. 2b). With this raster-type geometry, TUF-IOBES is capable of simulating the temperature and heat flux on the surface of each patch. Applying these TUF-IOBES boundary conditions in PALM makes it possible to simulate the effects of the realistic temperature distribution on the flow pattern and heat transport in the canopy. Aside from analyzing general flow characteristics in 3-D urban canyons, the following processes and parameters are examined using the coupled model: (i) heterogeneous insolation during the day, (ii) different urban materials (windows versus walls and different street surface albedo) (iii) different stability conditions through variable wind speed.

### 2.1 Simulation Set-Up in TUF-IOBES

The physical building set-up and thermal properties of the construction materials are post-1980 buildings that satisfy insulation requirements for non-residential buildings in ASHRAE 90.1-2004 (American Society of Heating, Refrigerating and Air-Conditioning Engineers Inc. 2004) (Table 1 in [Yaghoobian and Kleissl 2012b](#)). Buildings have square footprints of 21.3

**Table 1** Stratification, ground surface albedo, and bulk wind speed for the August 17 and June 9 PALM simulations

Day	Stratification	Canopy floor albedo	Wind speed ( $\text{m s}^{-1}$ )
Aug 17	Unstable	0.1	1.8
Aug 17	Unstable	0.5	1.8
Aug 17	Unstable	0.1	0
Aug 17	Unstable (with uniform surface heat fluxes)	0.1	1.8
Aug 17	Neutral	–	1.8
Jun 9	Unstable	0.1	3.7
Jun 9	Unstable	0.5	3.7
Jun 9	Neutral	–	3.7

The base case is shown in *italics*

m on each side and heights of 18.3 m; each wall of the buildings has a window centered on the wall with dimensions of 12.2 m height  $\times$  15.2 m width resulting in a window fraction of 0.47. Windows are triple-pane clear 1 Low-E layer that were chosen to meet ASHRAE Standard 90.1-99. All surfaces in the TUF-IOBES geometry are divided into patches with 3.05 m length on each side. A detailed description of thermal and radiative properties of the construction materials can be found in Sect. 2 of [Yaghoobian and Kleissl \(2012b\)](#). Simulations were performed for a domain of  $5 \times 5$  identical building with a canopy aspect ratio (building height to the distance between buildings) of unity in both horizontal directions. Two clear summer days, June 9 with moderate average wind speed of  $3.7 \text{ m s}^{-1}$  and August 17 with a low average wind speed of  $1.8 \text{ m s}^{-1}$  were chosen from the TMY3 weather data file of the Phoenix Sky Harbor International airport ( $33.45^\circ\text{N}$ ,  $111.983^\circ\text{W}$ , and 337 m altitude) in Arizona, USA. For each of these days, simulations were performed for canopy ground albedos of 0.1 and 0.5 (weathered asphalt and white Portland cement concrete, respectively; American Concrete Pavement Association, 2011), while the building wall and roof albedos were kept constant at 0.3 and 0.6, respectively. As expected, the temperature of the darker ground surface was significantly higher than the temperature of the brighter surface. However, the larger shortwave reflection of the brighter surface increased surface temperatures of the outdoor building walls and window transmission. Therefore buildings near bright street surfaces were associated with larger cooling loads; for details see [Yaghoobian and Kleissl \(2012b\)](#).

## 2.2 Domain Size and Grid Sensitivity and Simulation Set-Up in PALM

Evidence of the correlation between the turbulent flow structure within a cubical canopy and the large organized structures of turbulence within the inertial sub-layer above (e.g. [Kanda et al. 2004](#); [Coceal et al. 2007](#); [Inagaki and Kanda 2010](#); [Takimoto et al. 2011](#); [Inagaki et al. 2012](#); [Perret and Savory 2013](#)) necessitates a preliminary sensitivity test for choosing the most appropriate computational domain size. In the [Inagaki et al. \(2012\)](#) simulation of a daytime atmospheric boundary layer over a large domain of regular array of cubes, the inertial sub-layer formed between heights of  $1.5H$  and approximately  $6H$  ( $H$  is the height of the cubes). The turbulent organized structures within this layer are several times  $H$  in the spanwise direction, and more than  $10H$  in the streamwise direction ([Inagaki et al. 2012](#)). A control simulation was performed for the building and canyon geometry described in Sect. 2.1 in a domain of 10 (streamwise) by 3 (spanwise) buildings resulting in a domain size of  $21.3H$

(length)  $\times 6.4H$  (width)  $\times 5H$  (height); the goal was to choose a domain much larger than the integral dimensions of the turbulent organized structures reported in Inagaki et al. (2012). The height of the domain for the control simulation ( $5H$ ) was chosen to be large enough to cover the inertial sub-layer in which the turbulent organized structures are located. Based on Inagaki et al. (2012) the inertial sub-layer for cube arrays forms at heights between  $1.5H$  and approximately  $6H$  and based on wind-tunnel experiments (Cheng and Castro 2002) it forms between  $1.8H$  and  $2.4H$ . Then the domain size was reduced and the similarity to the control case was examined using a grid spacing of  $0.03H$ . Based on a comparison of time- and ensemble-averaged profiles of velocity components, temperature, SGS TKE, and velocity variances (not shown) a computational domain of  $10.6H$  (length)  $\times 6.4H$  (width)  $\times 5H$  (height) (5 by 3 buildings) was found to yield sufficiently similar results as the largest (control) domain size.

To choose an appropriate computational resolution a grid independency analysis was conducted, where three simulations were performed in which the cubical canyons in the domain were resolved by 20, 32, and 40 grids (respectively representative of grid sizes of  $0.05H$ ,  $0.03H$ , and  $0.025H$ ). Comparison of time- and ensemble-averaged profiles of velocity components, temperature, SGS TKE, and velocity variances (not shown) indicate that a moderate resolution with grid spacing of  $0.03H$  yields the best compromise between accuracy and computational cost.

The grid spacing is uniform in the horizontal directions, and in the  $z$  direction, the grid spacing is uniform up to  $z = 3H$  and then gradually increases with an expansion ratio of 1.08. Due to the use of uniform grids, the building size in TUF-IOBES (21.3 m (length)  $\times$  18.3 m (height)) was modified to 21.05 m  $\times$  18.57 m. This modification is less than 0.27 m (1.4%) and has negligible effects on the aggregated emitted heat flux from the building surfaces. In the horizontal directions boundaries are periodic resulting in an infinite homogeneous urban surface boundary. At the top boundary, a zero-gradient (free-slip) boundary condition is used for momentum that has effects similar to those of a strong inversion (Shaw and Schumann 1992). The temperature at the domain top is specified to be constant (see Sect. 2.4), and the direction of the flow in all simulations is from west (left) to east (right). Coriolis forces are not considered.

### 2.3 Model Coupling

One-way coupling is implemented whereby surface convective heat fluxes (not the surface temperatures) simulated in TUF-IOBES are used as thermal boundary conditions for all solid surfaces in PALM. While two-way coupling between the flow field in PALM and conduction and radiation heat transfer in TUF-IOBES could provide the most realistic surface temperature distribution and fluid flow, radiation effects dominate the surface temperature heterogeneity (e.g. Yaghoobian et al. 2010). The complexity of integrating these codes cause us to leave two-way coupling to future work. The surface convective heat fluxes in TUF-IOBES are simulated based on the temperature differences between surfaces and canopy air multiplied by a convective heat transfer coefficient based on an empirical model known as the DOE-2 method (LBL 1994). The alternative approach, computing heat fluxes dynamically in PALM using a wall function method and surface temperatures from TUF-IOBES, was rejected because the TUF-IOBES energy conservation is violated.

The TUF-IOBES patch heat fluxes over square patches of 3.05 m length are bilinearly interpolated to heat fluxes over PALM grids with 0.62 m length on each side. In addition PALM is modified to allow heterogeneous gridded heat fluxes. The TUF-IOBES patch surface heat fluxes are available every 15 min and linearly interpolated to the PALM timestep,

allowing the simulation of the effects of gradual shadow movements and associated surface heat fluxes on clear days on the flow and heat transport in the urban canopy.

## 2.4 Suite of Simulations

Since the thermal boundary conditions are from the TUF-IOBES simulations of June 9 and August 17 in Phoenix, Arizona, the initial ambient bulk wind velocity in the PALM simulations (Table 1) is set to the average wind speed of these days from TMY3 weather data for Phoenix ( $3.7$  and  $1.8 \text{ m s}^{-1}$ , respectively). Temperature results are very sensitive to the temperature boundary condition at the top of the domain, and several tests showed that if the TMY3 mean air temperature between 0300 and 2000 LST (the time period that was chosen for the PALM simulation; see below) was used as the upper boundary condition, the average canopy air temperature was within  $2\text{--}3^\circ\text{C}$  of the simulated canopy air temperature in the TUF-IOBES simulations throughout the day. Therefore at the top of the domain the temperature is set to  $31.7$  and  $33.2^\circ\text{C}$  for June 9 and August 17, respectively.

Since nighttime surface temperatures are more homogeneous in the canopy we focus on the daytime. Each simulation was performed from 0300 to 2000 LST in which the first 6 h were considered as the spin-up period. Simulation fields were averaged over consecutive 1,800 s intervals. For reference, a free convective (zero wind speed, August 17) and two neutrally stratified simulations (i.e. the surface temperatures at the street, wall and roof are the same as the (homogeneous) air temperature) were performed with initial bulk wind speeds of  $1.8 \text{ m s}^{-1}$  (August 17) and  $3.7 \text{ m s}^{-1}$  (June 9). Each of these neutral simulations was conducted for 7 h and the last 1,800 s were used for analysis. For neutral conditions the time period of 1,800 s corresponds to at least 12 eddy turnover times of the primary circulation in the canyon,  $t_c = H/U_c$ , where  $U_c$  is the mean scalar wind speed in the canyon.

## 3 Validation

The TUF-IOBES validation is described in [Yaghoobian and Kleissl \(2012a\)](#). In [Park et al. \(2012\)](#) the velocity and temperature fields of PALM in a bottom-heated street canyon are validated against the wind-tunnel data of [Uehara et al. \(2000\)](#). In the present study PALM is validated against data from the wind-tunnel experiment of [Kovar-Panskus et al. \(2002\)](#) for a 2-D street canyon with heated windward wall and canyon aspect ratio (height to width) of 1.0. The street canyon is represented by a cavity with dimensions  $H \times H \times 4H$  (LES) and  $H \times H \times 8.8H$  (wind tunnel) in the centre of the domain (see Fig. 1 in [Kovar-Panskus et al. 2002](#)); the PALM domain width and height are  $4H$  and  $5H$ , respectively. Note that in PALM the cyclic wind and temperature boundary conditions mimic an infinite number of infinite street-canyon cavities spaced by  $5H$  in the streamwise direction. On the other hand, the wind-tunnel experiment is composed of a single 2-D canyon cavity.

As with the wind-tunnel experiment, the Reynolds number  $Re \sim 10^4$  in the LES. Use of  $Re$  is one of the principal similarity criteria when comparing a wind-tunnel experiment and a numerical simulation. However, as stated by [Allegrini et al. \(2013\)](#) for flow around bluff bodies,  $Re$  similarity is not required; the Reynolds number only needs to be larger than a critical value to guarantee Reynolds-number independent flow. Along these lines, in the validation of [Cai \(2012\)](#) using the same wind-tunnel experiment, he assumed that for his LES  $Re \sim 10^4\text{--}10^6$  was large enough to be in the flow regime that is independent of Reynolds number. Since our initial validation for the neutral case using  $Re \sim 10^6$  (not shown) showed a significant difference in the LES mean flow field from  $Re \sim 10^4$ , we hypothesize that

$Re \sim 10^4$  is below the critical Reynolds number for this flow. However, Reynolds number dependence may also be attributed to shortcomings of the SGS scheme or insufficient spatial resolution.

The mean canopy flow fields at different Froude numbers ( $Fr$ ) were compared against the wind-tunnel experiment, where different surface heat fluxes were prescribed at the windward wall to vary the Froude number,  $Fr = U_{\text{ref}}^2 / (gH(T_{\text{wall}} - T_{\text{ref}}) / T_{\text{ref}})$ , where  $H$  is the canyon height,  $g$  is the acceleration due to gravity,  $T_{\text{wall}}$  is the wall surface temperature, and  $U_{\text{ref}}$  and  $T_{\text{ref}}$  are the ambient, freestream wind velocity and temperature. To calculate  $T_{\text{wall}}$ , the relation  $Q_h = h(T_{\text{wall}} - T_{\text{air}})$  was used in which  $Q_h$  is the prescribed wall heat flux,  $h$  is the convective heat transfer coefficient simulated based on the DOE-2 method, and  $T_{\text{air}}$  is the simulated air temperature at the first grid point near the windward surface. To calculate  $h$ , the volumetric mean scalar wind speed and mean air temperature inside the canopy simulated in PALM were used as the environmental wind speed and air temperature in the DOE-2 method (details of the DOE-2 method are presented in the Appendix). While the DOE-2 method is not commonly applied to determine  $T_{\text{wall}}$ , it is consistent with the obtaining of convective fluxes in TUF-IOBES. Therefore the validation extends beyond testing PALM also to the coupling with TUF-IOBES.

Figure 1a, b shows mean velocity vectors of the LES side-by-side with the wind-tunnel experiment of Kovar-Panskus et al. (2002) for  $Fr=0.73$ . The location of all three vortices at the top, bottom left and bottom right of the canyon in the PALM simulation are comparable to those in the wind-tunnel experiment. For  $Fr = 1.17$  (Fig. 1c, d) again, the features of the flow are very similar. For example the velocity vectors at the top of the canopy show the same pattern without updraft despite the heated wall. Also the size of the vectors in the LES and the wind-tunnel results shows that the downward wind speed near the windward wall is much larger than the upward wind speed near the leeward wall. Similarly, as in the validation results of Cai (2012) the primary vortex is shifted to the right (Fig. 7a in Cai 2012), which differs from the location of the ‘sketched’ primary vortex in the experimental results. We believe that the sketched vortex does not provide the correct aspects of the physical process. The shape and magnitude of the mean velocity vectors that are similar in both Fig. 1c, d suggest that, based on mass conservation (downward mass flux into the canyon near the windward wall equals the upward mass flux out of the canyon near the leeward wall) the primary vortex should be shifted to the right, as in the LES results of Cai (2012) and PALM. As argued by Cai (2012) the flow pattern in the experiment results can only be explained by either an undetected strong updraft near the leeward wall or a mass divergence along the canyon axis. Neither feature was discussed by Kovar-Panskus et al. (2002) and this aspect of the experimental results remains questionable. Overall the validation can be considered to be successful.

## 4 Results and Discussion

Since this study involves investigating the effects of diurnal canyon surface heating on flow and heat transport in *three-dimensional* street canyons, it is necessary to consider both spanwise and streamwise canyons (Fig. 2a) in explaining the results. Unless stated otherwise, all results are time-averaged over 1,800 s and ensemble-averaged over the canopies in the domain (all spanwise (streamwise) canyons are used for calculating the ensemble-averaged spanwise (streamwise) canyon). Figure 2b shows the surface temperature of walls, windows, rooves and ground in the TUF-IOBES simulation domain at 1015, 1315, 1615, and 1915 LST August 17 in Phoenix, Arizona where the ground surface albedo is 0.1. Figure 2b illustrates

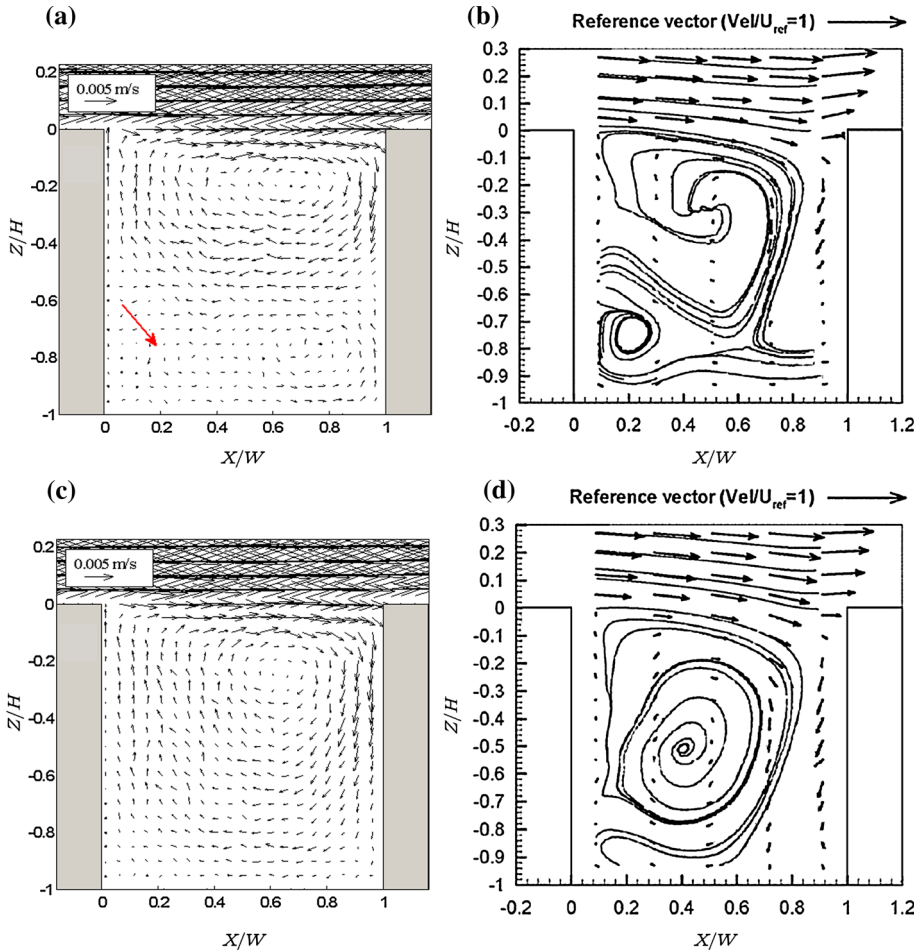


**Fig. 1** Simulated mean wind field in PALM with  $Fr = 0.73$  (a) and  $1.17$  (c), and mean velocity vectors and streamlines of Kovar-Panskus et al. (2002) for cases with  $Fr = 0.73$  (b) and  $1.17$  (d). The windward (right) wall is heated. The red arrow in (a) shows the location of the bottom left vortex

the dynamic thermal forcing that will later be shown to cause variations of flow in urban canopies.

In all plots of mean flow, temperature, and pressure fields, the building (canyon) width is enlarged (reduced) by  $\Delta x/H$  compared to the actual non-dimensional building (canyon) width ( $\Delta x$  is the grid spacing). This modification was introduced for aesthetic reasons and due to the staggered grid in PALM.

#### 4.1 Mean Flow and Temperature Field in the Spanwise Canyon

Due to the high solar altitude and the east-west orientation of the streamwise canyon most of the ground surface in the streamwise canyons (which are located between north and south facing walls) receives direct solar radiation throughout the day; only the north facing walls are shadowed (Fig. 2). Therefore velocity and temperature fields for the streamwise canyons



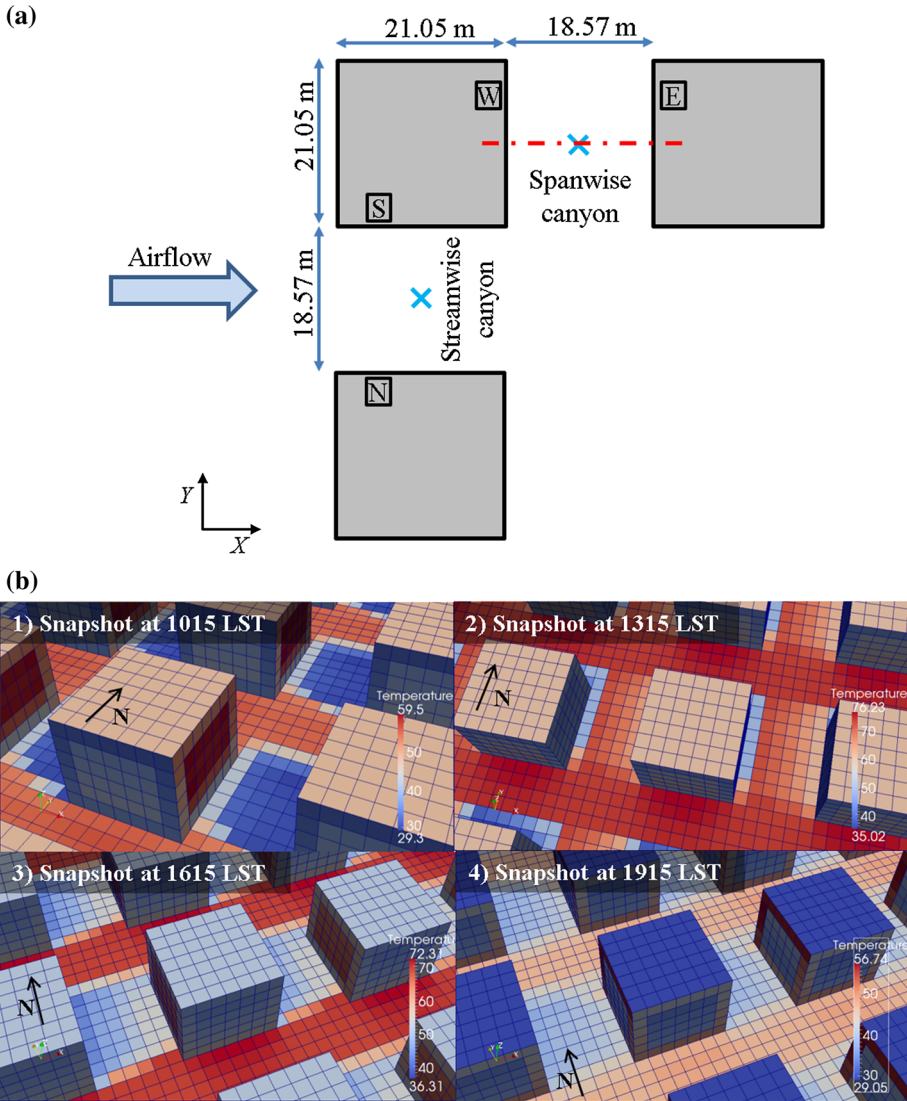


**Fig. 2** a Plan view of three (out of 15) buildings showing streamwise and spanwise canyons in the PALM domain. Square boxes next to each wall indicate the aspect of the building walls. The red dashed line is the location of the vertical cross-section at the centre of the spanwise canyon in Figs. 3, 10, 12, and 13. Blue crosses are the centres of the spanwise and streamwise canyons in Figs. 4 and 6, respectively. b Surface temperature in the TUF-IJBES simulation domain at (1) 1015, (2) 1315, (3) 1615, (4) 1915 LST of the August 17 simulation with ground surface albedo of 0.1 in Phoenix, Arizona (the base-case simulation). The length of each patch is 3.05 m and the centre 4 × 5 patches of each facet are windows with different thermal properties than the surrounding wall area. The direction of the flow is from west to east

are not shown since the relative thermal forcing from the streamwise canyon surfaces does not change significantly throughout the day; the ground is the warmest surface while the north facing wall is the coolest.

Instead, Fig. 3 shows the spatial distribution of the time- (1,800 s) and ensemble-averaged velocity vectors and temperature in vertical and horizontal cross-sections in the middle of the

spanwise canyon for the August 17 simulation with a ground surface albedo of 0.1 (the base case) and for four different times of day, late morning (1000–1030 LST), early afternoon (1300–1330 LST), late afternoon (1600–1630 LST) and early evening (1900–1930 LST). Averaged heat flux from all surfaces of the spanwise canyon over the canyon floor area, averaged friction velocity, and bulk Richardson number for the chosen time spans in the spanwise canyon of the base case are presented in Table 2. The bulk Richardson number  $Ri = (g/T_H)((T_H - T_0)/H)(u_H/H)^{-2}$ , where  $T_H$  and  $u_H$  are mean canyon temperature and horizontal wind speed at the roof level, and  $T_0$  is the air temperature averaged over the closest grid points to the ground surface.  $Ri$  is calculated from the ensemble- and time-averaged fields in the spanwise canyon.

The ensemble mean velocity vectors in the vertical cross-section (left column in Fig. 3) show a dominant canyon vortex centered at a constant height (around  $z/H = 0.75$ ) throughout the day. The persistent location and speed of the canyon vortex suggests that the mechanical force and the horizontal streamwise thermal force induced by the temperature (and as

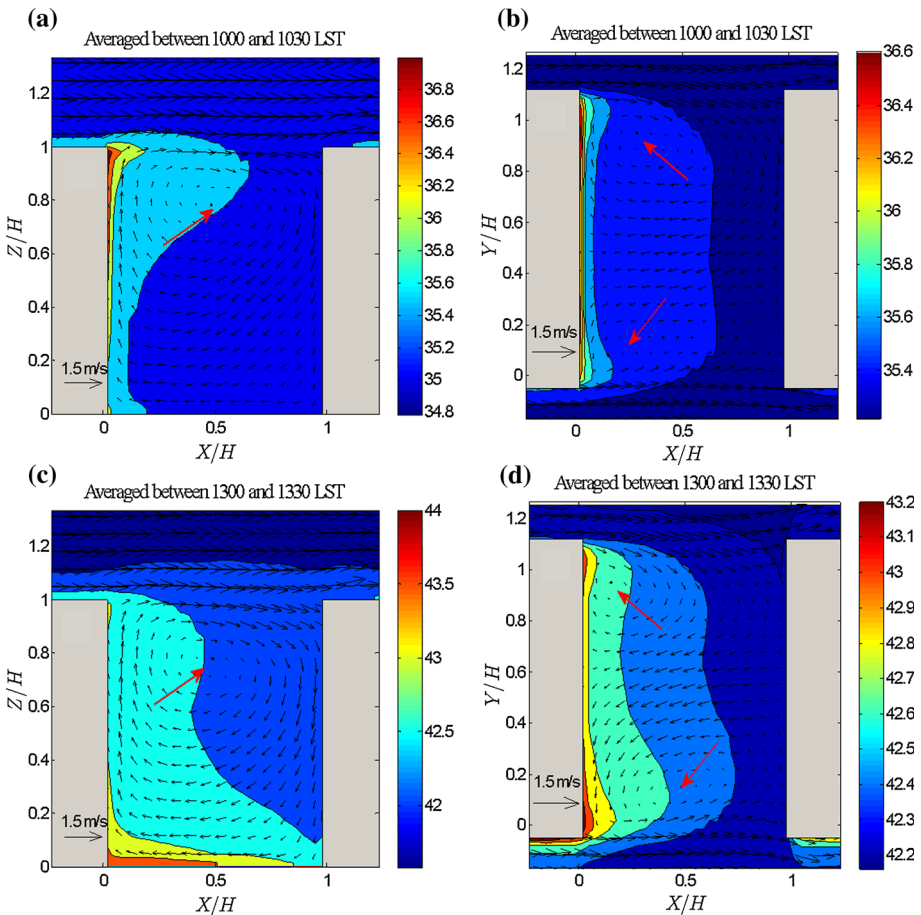


**Fig. 3** Ensemble- and time-averaged velocity vectors and temperature field in vertical (left column) and horizontal (right column) cross-sections in the middle of the spanwise canyon of the base case simulation. The red arrows mark vortex centres

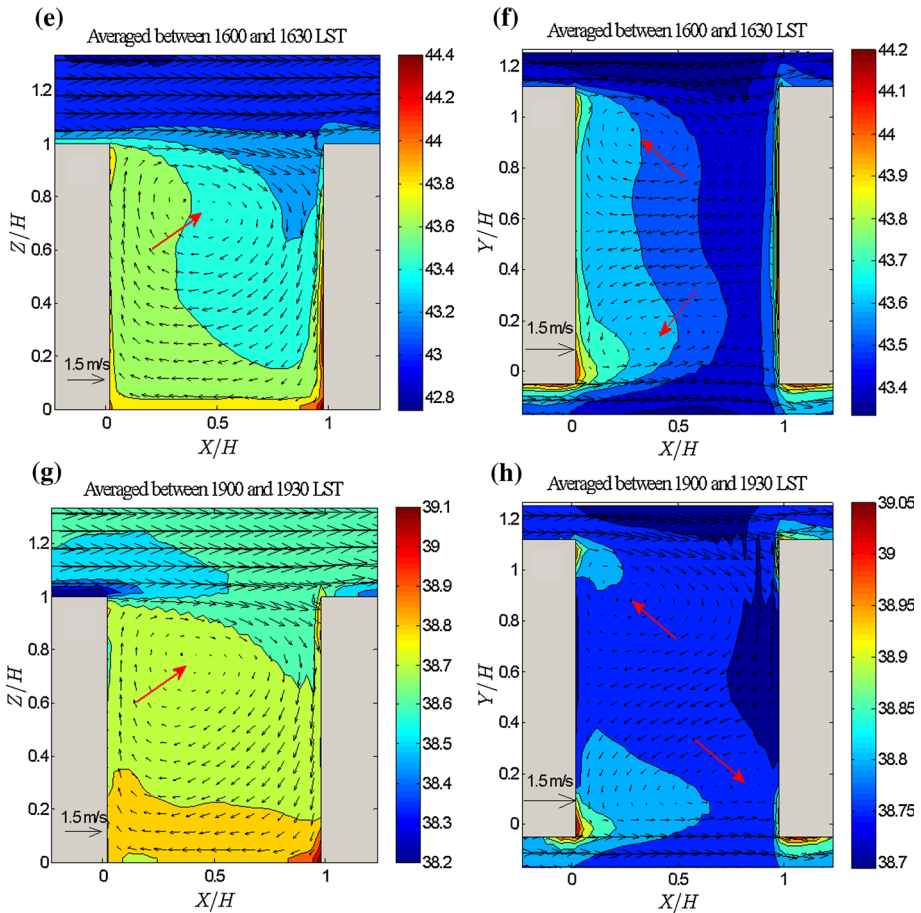


**Fig. 3** continued

**Table 2** Averaged heat flux from all surfaces in the spanwise canyon over the canyon floor area ( $\text{W m}^{-2}$ ), averaged friction velocity, and bulk Richardson number in the spanwise canyon of the base case

	1015 LST	1315 LST	1615 LST	1915 LST
Total heat flux ( $\text{W m}^{-2}$ )	36.8	150.6	200.1	92.9
Friction velocity ( $\text{m s}^{-1}$ )	0.12	0.14	0.13	0.1
Bulk Richardson number	0.37	-1.58	-0.73	-0.33

a result pressure) difference between the air right above the roof surfaces and above the spanwise canyon outweigh the thermal forces from the heated surfaces inside the canyon in defining the general flow pattern in the spanwise canyon. For instance, thermal forcing from the heated downwind wall in the late afternoon and early evening are insufficient to produce an updraft to reverse the clockwise canyon vortex. These results are consistent with observations of previous atmospheric (e.g. Louka et al. 2002; Offerle et al. 2007; Idczak et al. 2007) and wind-tunnel (e.g. Richards et al. 2006) experiments. In fact, the thermal forcing

from the heated building walls (and also rooves) strengthens the mechanically induced vortex throughout the day compared to the neutral simulation with bulk wind speed of  $1.8 \text{ m s}^{-1}$  (not shown here).

Two counter-rotating vortices are visible throughout the day in the horizontal cross-section (right column in Fig. 3) in the middle of the spanwise canyon. Due to the uneven thermal forcing caused by the partially shaded surfaces in the canyon and the temperature difference between windows and building walls these vortices are not symmetric. Heat from the south-facing walls, which are warmer throughout the day, is advected to the southern part of the spanwise canyon. This may explain the growth of the southern vortex in the spanwise canyon from morning to the evening compared to the northern vortex. The non-uniform thermal forcing of the wall surfaces is most noticeable between 1900 and 1930 LST (Fig. 3h). Due to higher pressure air adjacent to the cooler window surface in the centre of the west facing wall, and lower pressure air near the southern building edges, the centre of the southern vortex moves to the south-eastern part of the spanwise canyon.

The air temperature field in the canyon is relatively homogeneous with at most a  $2^\circ\text{C}$  temperature difference. Heating of the windward wall in the afternoon results in the most efficient mixing of heat throughout the canyon.

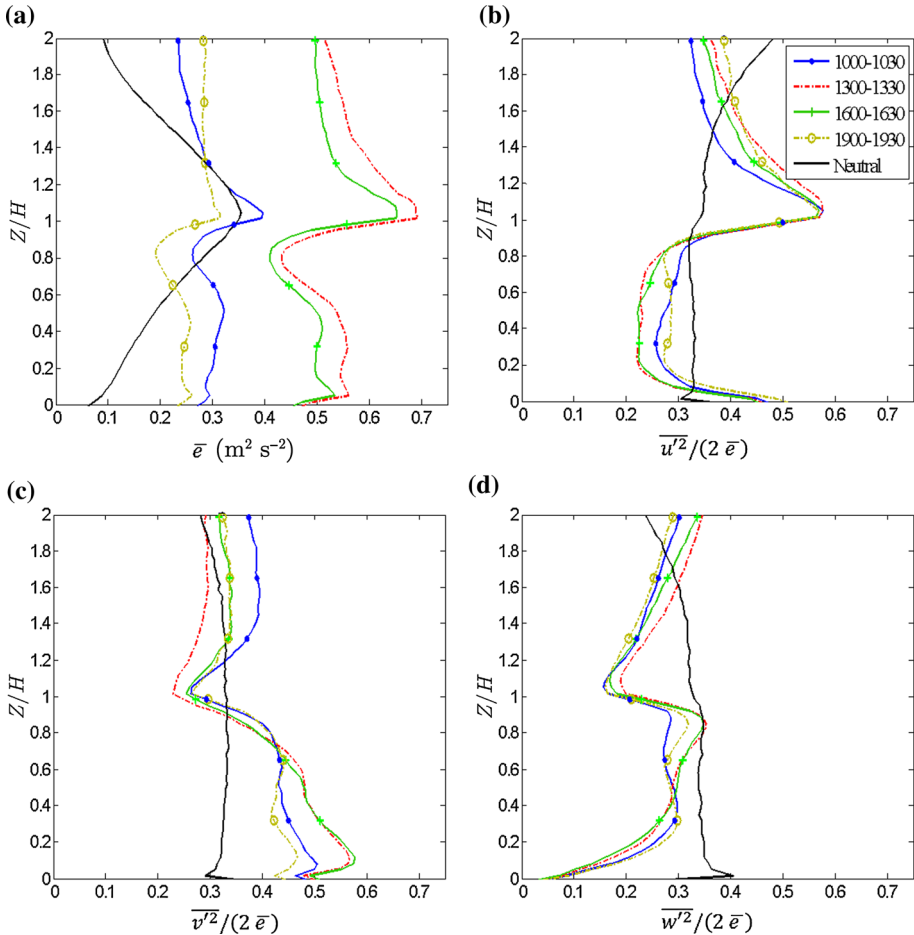
#### 4.2 Turbulent Kinetic Energy, Turbulent Fluxes, and Dynamic Pressure in Spanwise and Streamwise Canyons

Figure 4 shows the vertical profiles of TKE ( $\bar{\epsilon}$ ), streamwise and spanwise horizontal velocity variances,  $\overline{u'^2}$  and  $\overline{v'^2}$ , and vertical velocity variance,  $\overline{w'^2}$ , from the centre of the spanwise canyon for different times of day. Here,  $u'$ ,  $v'$  and  $w'$  are the velocity fluctuations obtained from a Reynolds decomposition of the filtered velocities at each grid point, i.e.  $u' = \bar{u} - \langle \bar{u} \rangle$  ( $\bar{u}$  is the instantaneous and  $\langle \bar{u} \rangle$  is the time-averaged filtered streamwise velocity). The SGS contributions are small and are ignored. The convective base case is compared to the neutral (no heating) case with identical wind forcing. To show relative contributions to the local TKE, the variances are normalized by twice the local TKE.

As is evident in Fig. 4a and consistent with previous studies (e.g. Cai 2012; Park et al. 2012), in *spanwise* canyons in both neutral and non-neutral cases TKE peaks at the roof height due to TKE production in the shear layer between the air and the roof surface, which is generated from a separation of the flow from the edge of the upstream building (Perret and Savory 2013).

Thermal forces modify the TKE in and above the canopies. As expected the TKE increases and decreases with the rise (morning to noon) and fall (noon to evening) of the thermal forcing (surface heat fluxes) during the course of the day. At 1915 LST, TKE at the rooftop is less than that in the neutral case because stable conditions above the roof surface (which cools radiatively at this time, Fig. 2b4) counteract the mechanical production of TKE. On the contrary, deeper inside the canopy where the surfaces are still warmer than the air due to the radiation trapping effect and release of stored heat, TKE is larger than for the neutral case.

Unlike the neutral case, profiles of TKE at different times of day in the non-neutral case have secondary peaks inside the street canyon. The TKE secondary peak shifts to the location of the warmest surface (corresponding to the location of more buoyant TKE production), which is the upper east facing wall at 1015 (Fig. 2b1) and the ground surface at 1315, respectively. This illustrates that the location of the TKE secondary peak in the canyon is related to non-uniform thermal forcing due to partially shaded surfaces and windows with different thermal properties than walls.



**Fig. 4** Vertical profiles of, **a** TKE ( $\bar{e}$ ), and relative contributions from, **b** streamwise horizontal, **c** spanwise horizontal, and **d** vertical velocity variances from the centre of the spanwise canyon of the base-case and neutral simulations. The variances are normalized by twice the local TKE. Besides ensemble and time averaging 9 ( $3 \times 3$ ) grid points in the centre of the canyon (rather than only one grid point) are averaged at each height to obtain the profiles

Figure 4b–d shows the fractional contribution of the horizontal and vertical velocity variances to the TKE in the centre of the spanwise canyon. In the neutral case the flow is more isotropic, i.e. all velocity variances equally contribute to the total TKE. On the other hand in the non-neutral simulations, the flow becomes strongly anisotropic. To investigate the forcing responsible for this strongly anisotropic behaviour of the flow we examine the pressure field in vertical cross-sections in the centre of the canyons. Generally pressure and velocity fields are dynamically linked (such as in Bernoulli’s equation or the Poisson equation for pressure fluctuations), but the heat flux from the canyon surfaces also modifies the pressure field by changing the density of air. Figure 5 shows the mean hydrodynamic (perturbation) pressure field ensemble- and time-averaged between 1600–1630 LST in  $x$ – $z$  and  $y$ – $z$  cross-sections in the middle of the spanwise canyon in neutral and non-neutral simulations.

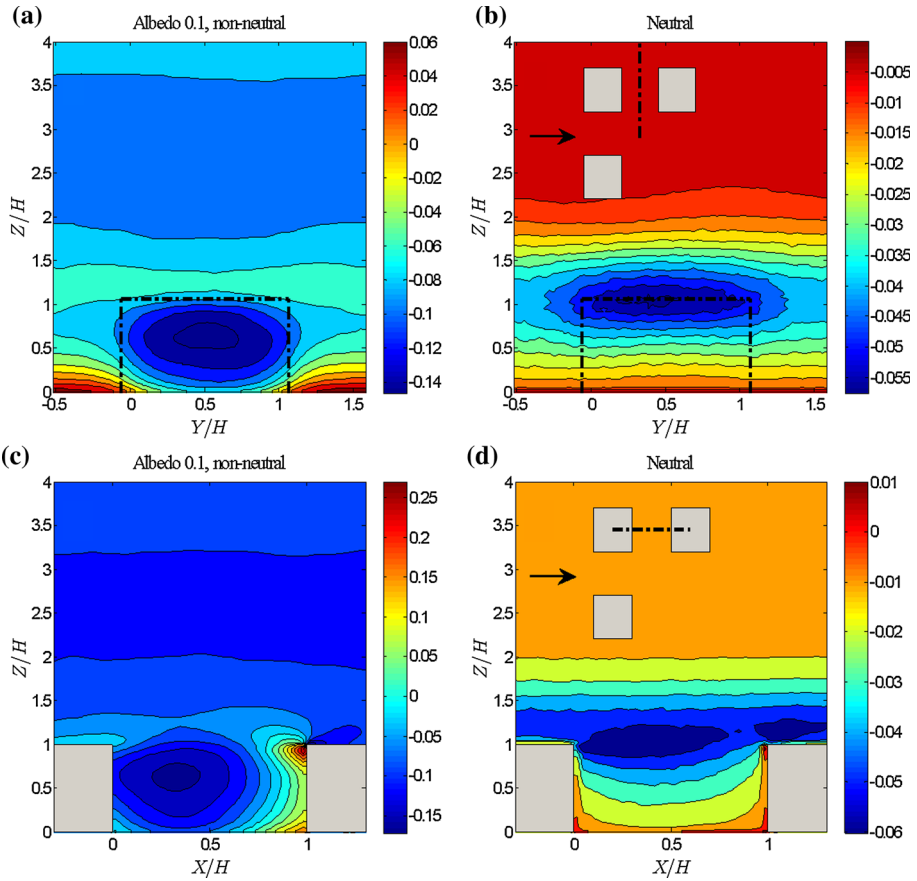


**Fig. 5** Ensemble- and time-averaged mean hydrodynamic pressure (Pa) field at 1600–1630 LST in  $y$ - $z$  (a, b) and  $x$ - $z$  (c, d) cross-sections in the centre of the spanwise canyon of the base case and neutral simulations. Refer to Fig. 2b3 for the surface temperatures for the base case at 1615 LST. Sketches of the buildings in (b, d) are in the  $x$ - $y$  plane and they respectively show the locations of the  $y$ - $z$  and  $x$ - $z$  cross-sections in the centre of the spanwise canyon

Figure 5a elucidates why the spanwise velocity variance,  $\overline{v^2}$ , is the main contributor to the TKE in the spanwise canyon. In the neutral case isosurfaces of mean pressure are aligned parallel to the ground surface (Fig. 5b) decreasing from the canyon floor (smallest velocity) uniformly up to the building height. At  $z = H$  the airflow separates at the upwind building edge and generates a boundary layer above the building roofs extending over the street canyon, consistent with a skimming flow pattern. Away from the roof surface, since the velocity converges to the bulk velocity, mean pressure increases gradually.

In the non-neutral simulation (Fig. 5a, c) because of stronger (thermally-driven) circulation (not shown) and the warm air trapped between the west-facing and east-facing walls, the low pressure area expands deeper inside the spanwise street canyon (Fig. 5a, c). Advection and vertical mixing cools the air over the street intersections, and consequently the air in these areas is cooler than the air inside the spanwise canyon (see the temperature field in the horizontal cross-sections of the spanwise canyon in Fig. 3). This creates a large horizontal pressure gradient in the spanwise ( $y$ ) direction (Fig. 5a), and is the main reason for the

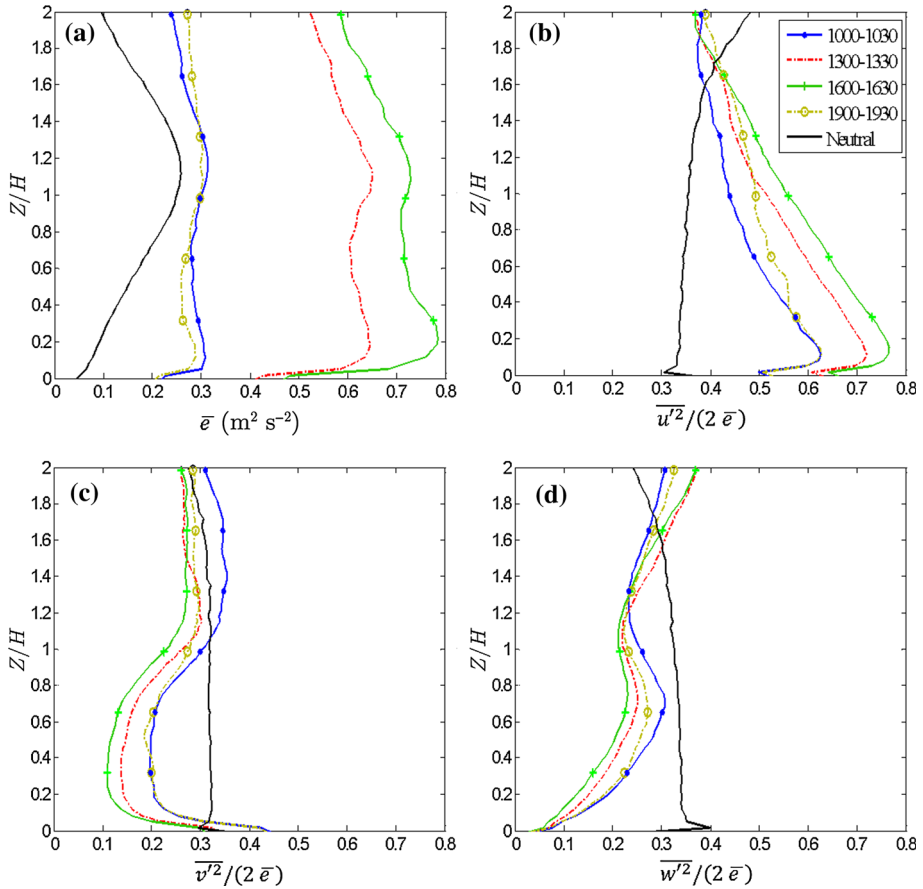


**Fig. 6** Vertical profiles of, **a** TKE ( $\bar{e}$ ), and relative contributions from, **b** streamwise horizontal, **c** spanwise horizontal, and **d** vertical velocity variances from the centre of the streamwise canyon of the base-case and neutral simulations. The variances are normalized by twice the local TKE. See the text for the averaging details

large contribution of  $\overline{v'^2}$  to the TKE in the spanwise canyons (Fig. 4c), which is enhanced near the ground where the largest spanwise horizontal pressure gradient exists (Fig. 5a). On the other hand, the air temperature immediately above the roof surfaces (which are continuously exposed to the sun during the day and cool radiatively at night) is significantly different than the air temperature at the same height over the top of the street canopies. This temperature difference generates horizontal pressure gradients in the non-neutral simulations (Fig. 5a, c). Consistent with the magnitude of horizontal temperature differences (around 0.4 °C difference, on average), at the roof level the streamwise horizontal pressure gradient is larger than the spanwise horizontal pressure gradient. Consequently, the streamwise velocity variance,  $\overline{u'^2}$ , contributes more to TKE (around 60 % of the total) than in the canopy. Although the amount of TKE in the spanwise canyon varies at different times of day (Fig. 4a), the relative contributions of the velocity variances to the total TKE do not change significantly with time (Fig. 4b–d). The reason is that the flow pattern in these canyons is mainly controlled by horizontal pressure differences (resulting from air temperature differences in the horizontal directions) that are relatively steady throughout the day. Minor differences can be detected for

more buoyant periods (at 1315 and 1615 LST) when the  $v$ -velocity contribution is enhanced near the surface and the  $w$ -velocity contribution is enhanced near the canopy top.

Figure 6 is the same as Fig. 4 but for the east-west oriented (streamwise) street canyon. In this canyon the larger TKE at the roof level of the neutral case is related to the shear layer and vortex shedding by the edges of the buildings lining the canyon. Again, thermal forces significantly increase TKE and anisotropy in the streamwise canyons, and TKE increases continuously from 1015 to 1615 LST. At 1915 LST, TKE inside the street canyon decreases but, unlike the spanwise canyon, remains larger than in the neutral case throughout the canyon depth.

Consistent with the canyon alignment, the contributions of the velocity variances to the TKE of the streamwise canyon (Fig. 6b–d) differ from that of the spanwise canyon (Fig. 4b–d). The variance  $\overline{v'^2}$  contributes less than in the neutral case and  $\overline{u'^2}$  contributes the most to TKE below roof level (50–60%).

Figure 7 is similar to Fig. 5 but for the streamwise canyon. The larger contribution of the streamwise velocity variance to the TKE in the non-neutral simulation is related to the larger streamwise pressure gradient (see Fig. 7a) induced by the temperature difference between the area in between the north-facing and south-facing walls and the cooler area over the intersection of the streets. Comparing Fig. 7a with b shows how thermal forcing modifies the isotropy of the flow compared to the neutral simulation. The contribution of  $\overline{u'^2}$  to the TKE varies noticeably with time of the day, much more so than in the spanwise canopies.

Generally in both streamwise and spanwise canyons the relative contribution of the vertical velocity variance to the TKE is less than for the neutral case. While a relative increase in horizontal velocity fluctuations with thermal forcing seems counter-intuitive, the pressure analysis supports the findings from the relative TKE profiles. It should be noted that, although the relative vertical velocity variance contribution to the TKE is less for buoyant production conditions than for neutrality, the actual values of the vertical variances are still higher for most heights under buoyant production conditions than for under neutral conditions.

Figure 8a, b (8c, d) shows the vertical profile of turbulent momentum (heat) fluxes,  $\overline{u'w'}$  ( $\overline{w'\theta'}$ ), for the spanwise and streamwise canyons, respectively. In the spanwise canyon, magnitudes of  $\overline{u'w'}$  at different times of day in the non-neutral simulation are up to 20 times those in the neutral case and peak at the rooftop level. Shear always causes large negative (downward)  $\overline{u'w'}$  at  $z = H$ , but the enhancement over neutral can be explained by the enhanced streamwise horizontal velocity above the roof surface due to the large streamwise horizontal pressure gradient at this location (Fig. 5c). The turbulent momentum flux,  $\overline{u'w'}$ , follows the diurnal cycle of surface thermal forcing increasing gradually from 1015 to 1315 LST and decreasing later at 1615 and 1915 LST. The turbulent momentum flux becomes positive (upward) below about  $0.6H$  because the spanwise canyon vortex, which is strengthened in the non-neutral case, causes a decrease in velocity magnitude with height. Since there is no comparable circulation in the streamwise canyons, the sign of the turbulent momentum flux is consistent (negative) at all heights but its magnitude varies with the magnitude of thermal forcing.

Due to the high TKE, large roof-surface heat flux, and also large air temperature gradient between inside and above the canopy, the vertical heat flux ( $\overline{w'\theta'}$ ) profiles in the centre of the spanwise canopy peak at roof level. Especially at roof height, the turbulent heat flux follows the diurnal cycle of the ground and roof-surface heat flux throughout the day. The large secondary peak near the ground in the 1315 LST profile of the spanwise canyon is related to the large surface heat flux at this time, while large areas of the ground are shaded



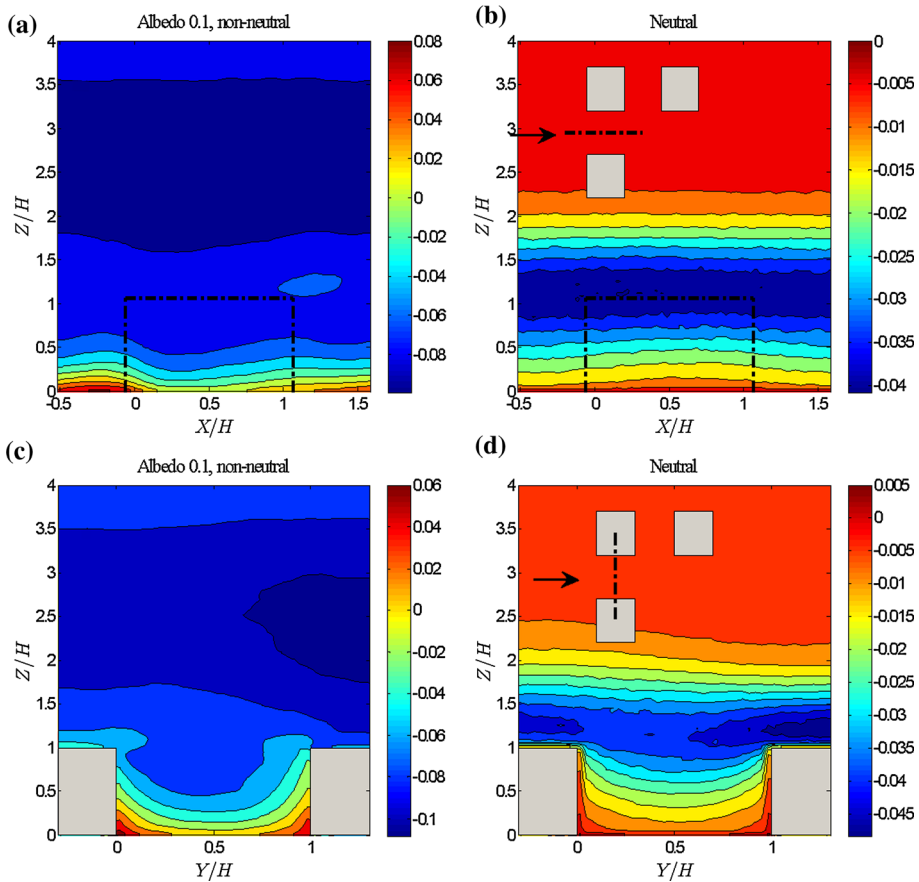


**Fig. 7** Ensemble- and time-averaged mean hydrodynamic pressure (Pa) field at 1600–1630 LST in  $x$ - $z$  (**a**, **b**) and  $y$ - $z$  (**c**, **d**) cross-sections in the centre of the streamwise canyon of the base case and neutral simulations. Refer to Fig. 2b3 for the surface temperatures for the base case at 1615 LST. Sketches of the buildings in (**b**, **d**) are in the  $x$ - $y$  plane and they respectively show the locations of the  $x$ - $z$  and  $y$ - $z$  cross-sections in the centre of the streamwise canyon

at 1015 and 1615 LST. Unlike the spanwise canyons, the turbulent heat-flux profiles in the streamwise canyons are more uniform from the ground to  $z = 2H$ .

#### 4.3 Non-Uniform Thermal Forcing Within Canyon Surfaces (Effects of Sunlit Versus Shaded Surfaces and Heterogeneous Material Thermal Properties)

To investigate effects of non-uniform thermal forcing of the canyon surfaces due to the existence of partially shaded surfaces and window versus wall surfaces with different thermal properties we contrast those results against a case with uniform surface heat fluxes. In this additional simulation (hereinafter referred to as ‘uniform thermal forcing simulation’) the heat flux of each surface (e.g. roof, west wall, etc.) is defined as the average heat flux of all the patches on the same surface for the base case. In other words, the spatial variation is described by six different heat-flux boundary conditions that were variable in time, but uniform across the face. The ensemble- and time-averaged (over 1,800 s) air temperature,

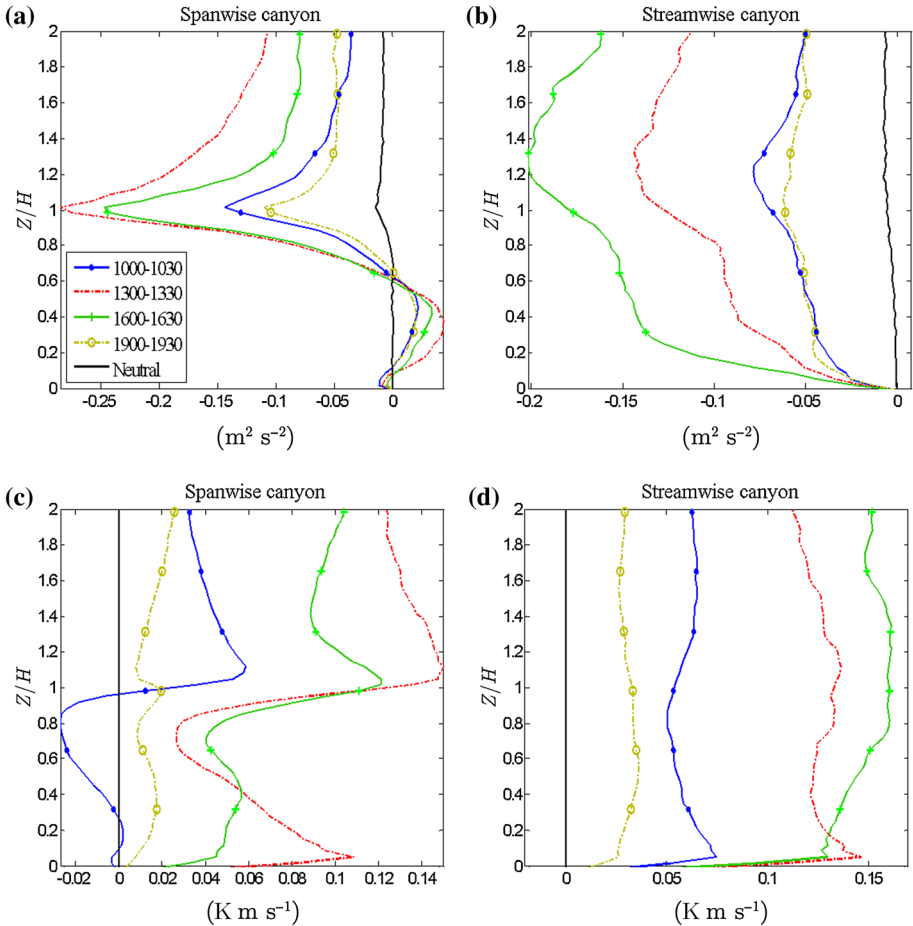


**Fig. 8** Vertical profiles of turbulent horizontal momentum and heat fluxes from the centre of the spanwise (*left column*) and streamwise (*right column*) canyons of the base-case simulation. Temporal and spatial averaging of these profiles are identical to those of TKE and velocity variances in Figs. 4 and 6

hydrodynamic pressure, and velocity magnitude of the base-case simulation from the time period between 1700 and 1730 LST are compared to those of the uniform thermal forcing simulation in a vertical and a horizontal cross-section in the centre of the spanwise canyon (Fig. 10). Figure 9 shows a snapshot of surface temperatures at 1715 LST from the base case TUF-IOBES simulation. Due to partial shading of the lower building walls and the near perpendicular solar incidence, this time period shows the largest within-surface temperature heterogeneity.

Figure 10a, b shows the mean temperature field difference between the uniform and non-uniform thermal forcing simulations. In general locally larger and smaller thermal forcing from the surfaces in the non-uniform simulation respectively generate lower and higher pressure compared to the uniform thermal forcing simulation. For example, the negative (positive) pressure difference adjacent to the upper (lower) part of the west facing wall in Fig. 10c can be explained by the higher (lower) air temperature in the non-uniform thermal forcing simulation (Fig. 10a) at this location. The air temperature difference is largest at

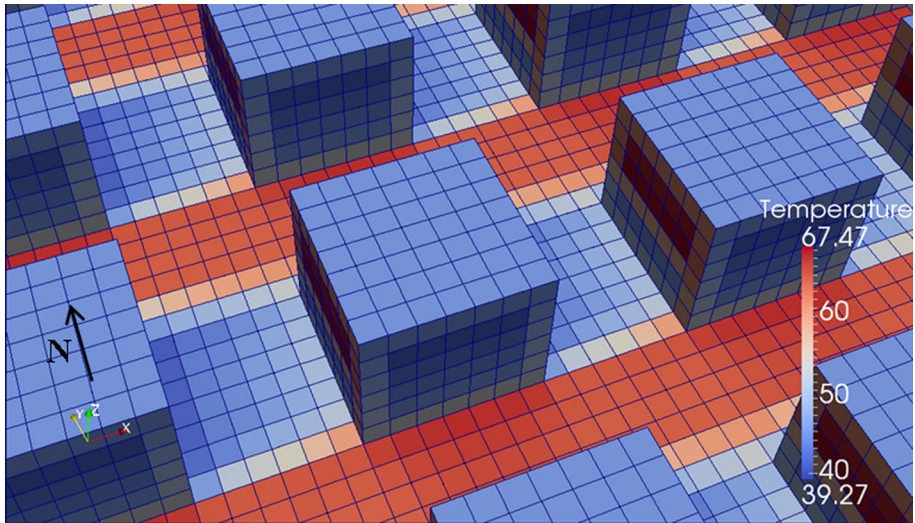


**Fig. 9** Surface temperature in the TUF-IOBES simulation domain at 1715 LST for the base-case simulation. The centre  $4 \times 5$  patches of each facet are windows. The direction of the flow in the PALM simulations is from west to east

the upper part of the windward wall, which receives direct solar radiation at near-normal incidence angles (Fig. 9). In Fig. 10d, the negative pressure difference in the southern part of the canyon is related to the warmer air in this area in the non-uniform simulation (Fig. 10b; also see Sect. 4.1). Figure 10e, f shows that generally the velocity magnitude locally increases and decreases respectively adjacent to the warmer and cooler spots in the non-uniform thermal forcing simulation compared to the uniform case. Comparison of the mean velocity *vector* fields of the uniform and non-uniform thermal forcing simulations (not shown here) shows no significant differences in the size and location of the main vortex in the vertical cross-section. This was predictable since, as mentioned in Sect. 4.1, the main factors in defining the size and location of the main vortex are the wind speed and the horizontal streamwise thermal force above roof level that outweigh the thermal forces from the heated surfaces inside the canyon. In the horizontal cross-section, the northern and southern vortices are symmetric in the uniform thermal forcing simulation whereas the southern vortex is larger in the non-uniform simulation.

#### 4.4 Ground Surface Albedo and Wind Speed

To holistically examine effects of the ground surface albedo and wind speed on flow characteristics and heat transport in street canyons a detailed 3-D investigation would be required. For conciseness, we focus on the effects of these parameters on the diurnal variation of canyon-averaged TKE while locally examining the mean temperature and velocity fields.

##### 4.4.1 Diurnal Variation of Canyon-Averaged TKE (Non-Local Effects)

Generally, the effects of ground surface albedo and wind speed change as a function of time of a day. Figure 11 shows the daytime (from 1000 to 1900 LST) variation of ensemble- and canyon-averaged TKE in the spanwise and streamwise canyons for all simulations.

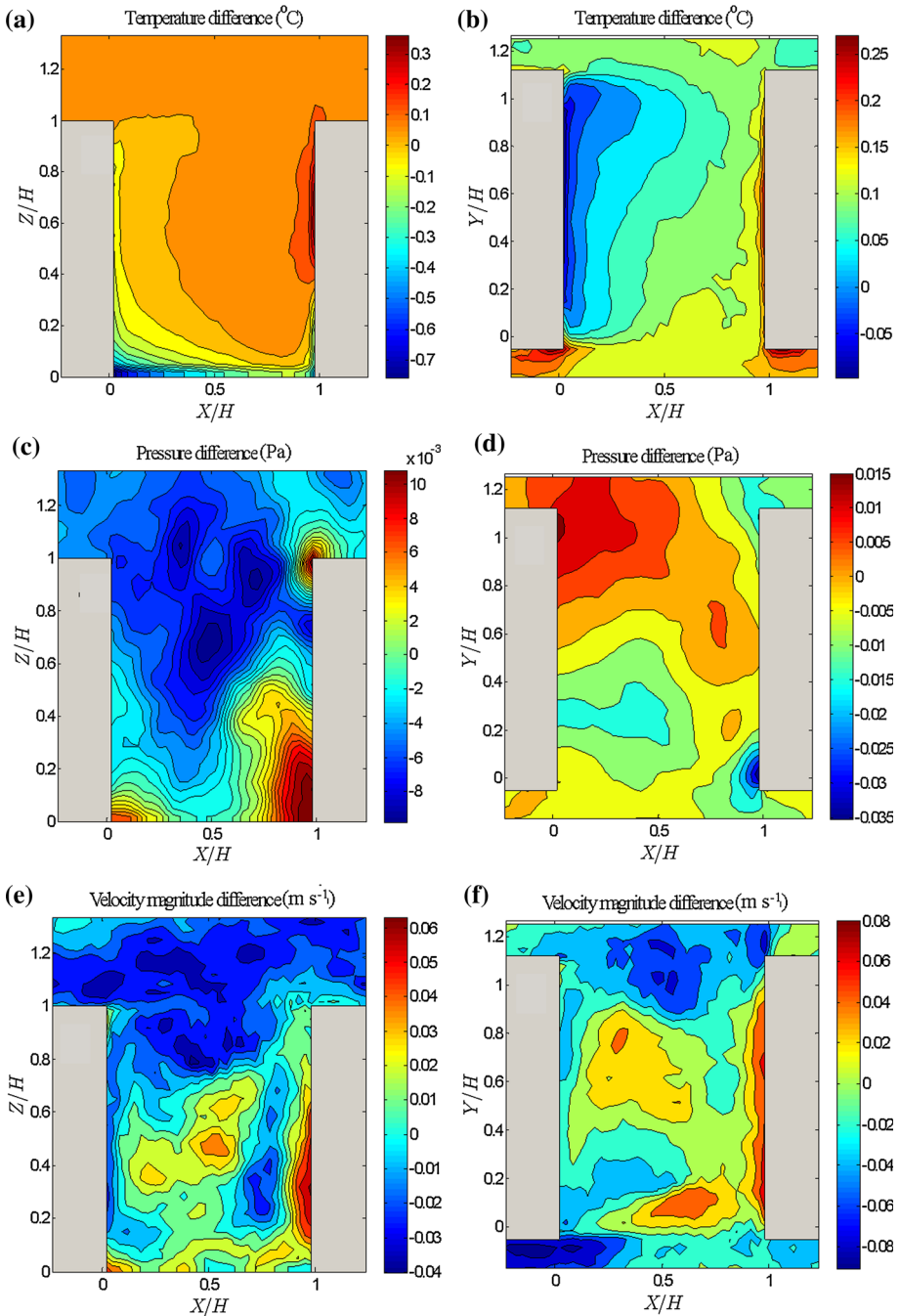


**Fig. 10** Ensemble- and time-averaged temperature (a, b), pressure (c, d) and velocity magnitude (e, f) difference of the base case simulation from the time period between 1700 and 1730 LST and the uniform thermal forcing simulation (see the text). The left (right) side panel is from a vertical (horizontal) cross-section at  $y/H(z/H) = 0.5$  of the spanwise canyon

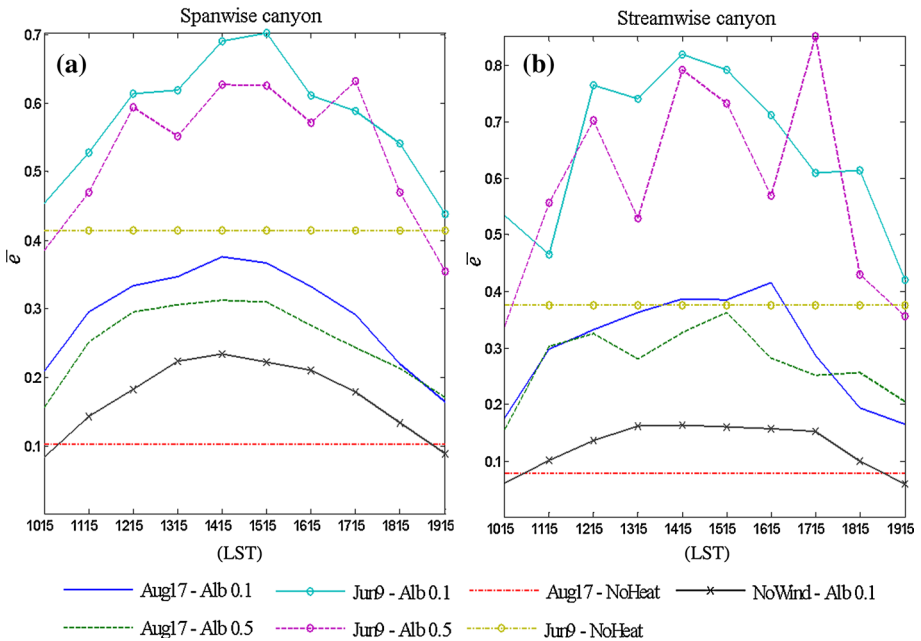


**Fig. 11** Ensemble-, time- and canopy-averaged TKE for, **a** spanwise, **b** streamwise canyons. Each marker represents a time-averaged value over 1,800 s. The ‘No wind\_alb 0.1’ case was run based on the August 17 thermal forcing. ‘NoHeat’ refers to neutral simulations

As expected the average TKE is larger on June 9 when the average bulk wind speed, and as a result the shear production, is larger. With the bulk wind speed of June 9 being twice that on August 17, the canopy-averaged TKE of the neutral simulation of June 9 is about four times that on August 17. Also, as expected, with thermal forces added the TKE inside the canyons increases and exhibits a diurnal cycle following the insolation on the ground surface in both canyons (Fig. 2b). Consistent with that trend, Fig. 11 shows that the street-canyon flow has greater TKE when the canopy-bottom surface is paved with darker materials and the ground surface temperature is higher as a result (Yaghoobian and Kleissl 2012b). From Fig. 11 it is also evident that the free-convection conditions (“NoWind”) generate larger values of TKE than for the pure mechanical forcing (“NoHeat”) on the weak wind day, but less than on the strong wind day. Interestingly the total is larger than the sum of its parts as the simulation with convection and mechanical forcing shows greater TKE than the sum of the neutral and free-convection simulations.

#### 4.4.2 Mean Temperature and Velocity Fields (Local Effects)

To illustrate the local effects of ground surface albedo and wind speed, the temperature and velocity magnitude difference between the low and high albedo simulations, and between the base case and no-wind case, are shown in Figs. 12 and 13, respectively. Velocity and temperatures are ensemble- and time-averaged between 1300 and 1330 LST when the ground surface in the spanwise canyon receives the most direct solar radiation.

Figure 12a shows that the air temperature inside the canyon of the low albedo base case is up to 2.5° C higher than for the high albedo case. Due to reduced shortwave reflection from

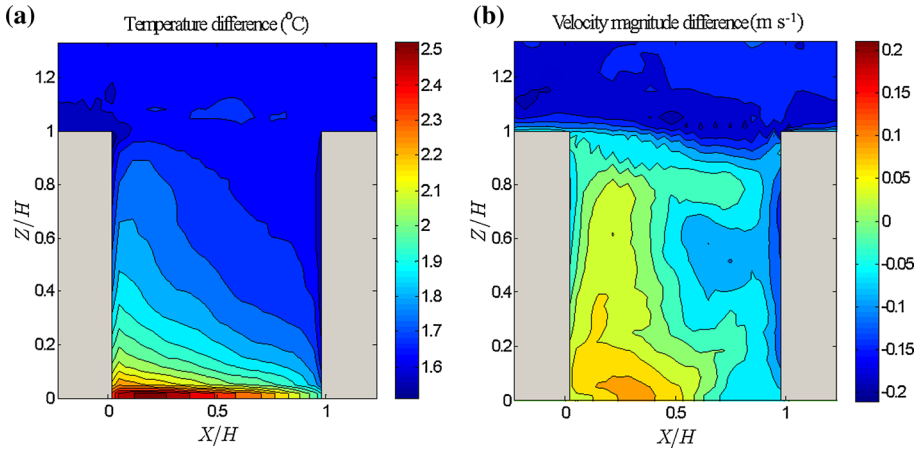


**Fig. 12** Ensemble- and time-averaged, **a** temperature, and **b** velocity magnitude difference of the base-case simulation minus the August 17 simulation with ground albedo of 0.5 averaged over 1300–1330 LST in a vertical cross-section at the centre ( $y/H = 0.5$ ) of the spanwise canyon

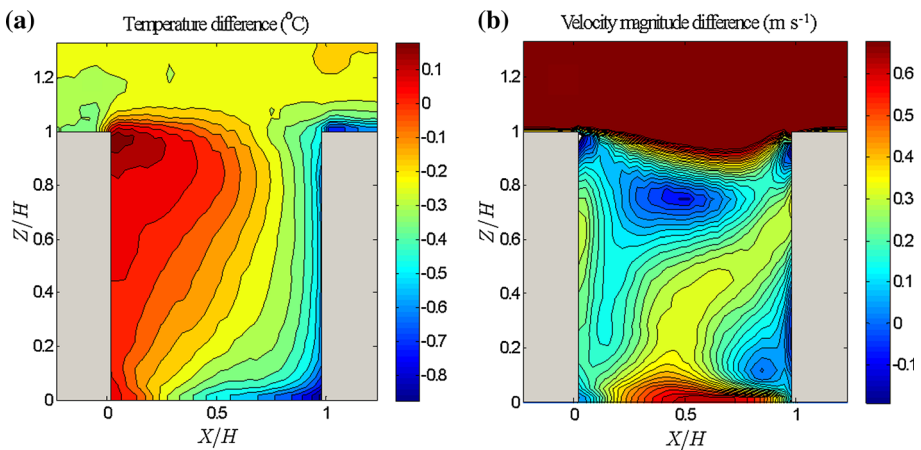


**Fig. 13** Ensemble- and time-averaged, **a** temperature, and **b** velocity magnitude difference of the base-case simulation minus the corresponding no wind simulation averaged over 1300 to 1330 LST in a vertical cross-section at the centre ( $y/H = 0.5$ ) of the spanwise canyon

the ground, with darker ground materials the surrounding building walls are cooler than with brighter ground materials (Yaghoobian and Kleissl 2012b) and a smaller air temperature increase is evident there. The velocity magnitude for the low albedo case is larger in the upwind part of the canyon since the thermal forcing is aligned with the direction of the canyon vortex there. The wind speed is smaller above the canyon due to the larger TKE and presumably stronger ejections and related shear driven by the stronger upward motion of the upwind half of the canyon vortex.

As expected, compared to the free-convection simulation the air is mixed more efficiently in the base case and therefore the air temperature inside the canopy is lower than in the free-convection case, except for within a short distance downwind of the roof (Fig. 13a). Not surprisingly, Fig. 13b shows that the velocity magnitude is larger in the mixed-convection

simulation of the base case than the free-convection simulation, and the difference is largest above the canopy. Comparison of the velocity vector field (not shown) illustrates that the negative velocity magnitude difference at  $z/H = 0.8$  marks the vortex centre in the base case simulation (where the velocity magnitude is small) whereas no vortical structure exists in the free-convection simulation.

## 5 Conclusions

In the daytime, urban canyon surfaces are heated by solar radiation. The amount of solar radiation received by the urban canyon surfaces is spatially and temporally variable throughout the canyon. The temperature of the surface primarily depends on the incident angle of direct solar radiation and on the thermal and radiative material properties. Despite the fact that the thermal forcing from urban surfaces is heterogeneous, most of the previous numerical studies represented urban areas through uniformly heated surfaces. In our study surface heat fluxes simulated in the Temperature of Urban Facets Indoor–Outdoor Building Energy Simulator (TUF-IOBES) were applied as thermal boundary conditions in the Parallelized Large-eddy Simulation model (PALM) to investigate the effects of urban materials with different thermal and radiative properties (e.g. windows versus walls, and reflective versus dark road pavements) and the moving shadows in the course of a day on the flow characteristics in a 3-D urban canyon. TUF-IOBES provides detailed surface-resolved thermal boundary conditions for CFD simulations. In addition, compared to several previous 2-D and 3-D numerical studies (e.g. [Kim and Baik 2010](#); [Kwak et al. 2011](#); [Cai 2012](#); [Li et al. 2012](#); [Park et al. 2012](#)), the larger domain size in the present study is expected to contribute to a more realistic representation of the effect of turbulent organized structures above the roughness layer.

The modified flow field of the non-uniform thermal forcing simulation compared to the uniform simulation demonstrates complex and temporally variable flow patterns induced by moving shadows and variable surface thermal properties, as evident, for example, from the location of the vortices in horizontal planes in the spanwise canyon.

Generally, spatial non-uniformity introduces horizontal pressure gradients in both streamwise and spanwise canyons throughout the daytime, and which generate larger fluctuations of the turbulent flow in the horizontal directions rather than in the vertical direction. Consequently passive scalars (e.g. pollution or water vapour) disperse more efficiently in the horizontal plane in between the canyons rather than being ventilated out of the canopies into the mixed layer. These pressure gradients are the results of air temperature differences in the spanwise and streamwise canyons as well as uneven input heat flux across each surface. This study demonstrates the importance of 3-D thermal boundary conditions and geometry to simulate the heat and mass transport in an urban area.

As an extension of this work, it would be of interest to study the effects of urban configurations with different street-canyon aspect ratios. Smaller aspect ratios result in the canyon vortices becoming less strongly expressed and may therefore be more sensitive to changes in horizontal pressure gradients. In addition, it would be desirable to study the diurnal variation of pollutant dispersion and human comfort in urban areas in the presence of detailed surface thermal boundary conditions. A two-way coupling between TUF-IOBES and PALM through simulating surface sensible heat fluxes in PALM, and applying them to simulate surface temperatures in TUF-IOBES, would provide more accurate flow and surface results.

**Acknowledgments** We would like to acknowledge the National Science Foundation CBET CAREER award 0847054 and high-performance computing support from Yellowstone (ark:/85065/d7wd3xhc) provided by NCAR's Computational and Information Systems Laboratory, sponsored by the National Science Foundation.

## Appendix: Description of the DOE-2 Method (LBL 1994; Pedersen et al. 2001)

The DOE-2 method calculates the convective heat transfer coefficient ( $h$ ) based on

$$h = h_n + R_f (h_{\text{glass}} - h_n), \quad (1)$$

for unstable flow,

$$h_n = 9.482 \sqrt[3]{|\Delta T|} / (7.238 - |\cos \phi|), \quad (2)$$

and for stable flow,

$$h_n = 1.81 \sqrt[3]{|\Delta T|} / (1.382 + |\cos \phi|). \quad (3)$$

Here  $h_n$  ( $\text{W m}^{-2} \text{K}^{-1}$ ) is the natural convection coefficient that is calculated from Eqs. 2 or 3,  $R_f$  is the surface roughness multiplier, and  $h_{\text{glass}}$  ( $\text{W m}^{-2} \text{K}^{-1}$ ) is the convection coefficient for very smooth surfaces (e.g. glass). In Eqs. 2 and 3,  $\Delta T$  is the temperature difference between the surface and air, and  $\phi$  ( $^\circ$ ) is the angle between the ground outward normal and the surface outward normal. Equations 2 and 3 are equivalent when the wall is vertical ( $\cos \phi = 0$ ). The surface roughness multiplier ( $R_f$ ) is based on the ASHRAE graph of surface conductance (ASHRAE 1981), where  $R_f$  is normalized to glass ( $R_f = 1$ ) and ranges up to 2.17 for stucco.  $R_f = 1.13$  for clear pine is used herein.

Here,  $h_{\text{glass}}$  is based on,

$$h_{\text{glass}} = \sqrt{h_n^2 + [aV_0^b]^2}, \quad (4)$$

in which constants  $a$  and  $b$  depend on the orientation of the surface with respect to the wind direction. For windward surfaces  $a = 2.38 (\text{W m}^{-2} \text{K} (\text{m s}^{-1})^b)$  and  $b = 0.89$  and for leeward surfaces  $a = 2.86 (\text{W m}^{-2} \text{K} (\text{m s}^{-1})^b)$  and  $b = 0.617$  (Yazdani and Klems 1994);  $V_0$  is the environmental wind speed.

## References

- Akbari H, Rainer L (2000) Measured energy savings from the application of reflective roofs in 3 AT&T regeneration buildings. Lawrence Berkeley National Laboratory, Paper LBNL-47075
- Allegrini J, Dorer V, Carmeliet J (2013) Wind tunnel measurements of buoyant flows in street canyons. *Build Environ* 59:315–326
- American Concrete Pavement Association (2011) Albedo: a measure of pavement surface reflectance. <http://www.pavement.com/Downloads/RT/RT3.05.pdf>. Accessed 15 Dec 2011
- American Society of Heating, Refrigerating and Air-Conditioning Engineers Inc. (2004) ANSI/ASHRAE/IESNA Standard 90.1-2004. Energy Standard for Buildings Except Low-Rise Residential Buildings I-P Edition
- ASHRAE (1981) 1981 ASHRAE Handbook—Fundamentals. American Society of Heating, Refrigerating, and Air-Conditioning Engineers Inc, Atlanta
- Berg R, Quinn W (1978) Use of light colored surface to reduce seasonal thaw penetration beneath embankments on permafrost. In: Proceedings of the second international symposium on cold regions engineering, University of Alaska, pp 86–99
- Boppa VBL, Xie ZT, Castro IP (2013) Large-eddy simulation of heat transfer from a single cube mounted on a very rough wall. *Boundary-Layer Meteorol* 147(3):347–368



- Bouyer J, Inard C, Musy M (2011) Microclimatic coupling as a solution to improve building energy simulation in an urban context. *Energy Build* 43:1549–1559
- Cai XM (2012) Effects of wall heating on flow characteristics in a street canyon. *Boundary-Layer Meteorol* 142(3):443–467
- Castillo MCL, Kanda M, Letzel MO (2009) Heat ventilation efficiency of urban surfaces using large-eddy simulation. *Ann J Hydraulic Eng* 53:175–180
- Cheng H, Castro IP (2002) Near wall flow over urban-like roughness. *Boundary-Layer Meteorol* 104(2):229–259
- Cheng WC, Liu CH, Leung DY (2009) On the correlation of air and pollutant exchange for street canyons in combined wind-buoyancy-driven flow. *Atmos Environ* 43:3682–3690
- Coccal O, Dobre A, Thomas TG, Belcher SE (2007) Structure of turbulent flow over regular arrays of cubical roughness. *J Fluid Mech* 589:375–409
- Deardorff JW (1980) Stratocumulus-capped mixed layers derived from a three-dimensional model. *Boundary-Layer Meteorol* 18:495–527
- Dimitrova R, Sini JF, Richards K, Schatzmann M, Weeks M, García EP, Borrego C (2009) Influence of thermal effects on the wind field within the urban environment. *Boundary-Layer Meteorol* 131(2):223–243
- Doulos L, Santamouris M, Livada I (2004) Passive cooling of outdoor urban spaces, the role of materials. *Sol Energy* 77:231–249
- Eliasson I, Offerle B, Grimmond CSB, Lindqvist S (2006) Wind fields and turbulence statistics in an urban street canyon. *Atmos Environ* 40:1–16
- Idczak M, Mestayer P, Rosant JM, Sini JF, Violleau MV (2007) Micrometeorological measurements in a street canyon during the joint ATREUS-PICADA experiment. *Boundary-Layer Meteorol* 124:25–41
- Inagaki A, Kanda M (2010) Organized structure of active turbulence over an array of cubes within the logarithmic layer of atmospheric flow. *Boundary-Layer Meteorol* 135:209–228
- Inagaki A, Castillo MCL, Yamashita Y, Kanda M, Takimoto H (2012) Large-eddy simulation of coherent flow structures within a cubical canopy. *Boundary-Layer Meteorol* 142(2):207–222
- Kanda M, Moriwaki R, Kasamatsu F (2004) Large-eddy simulation of turbulent organized structures within and above explicitly resolved cube arrays. *Boundary-Layer Meteorol* 112:343–368
- Kim JJ, Baik JJ (1999) A numerical study of thermal effects on flow and pollutant dispersion in urban street canyons. *J Appl Meteorol* 38:1249–1261
- Kim JJ, Baik JJ (2001) Urban street-canyon flows with bottom heating. *Atmos Environ* 35:3395–3404
- Kim JJ, Baik JJ (2010) Effects of street-bottom and building-roof heating on flow in three-dimensional street canyons. *Adv Atmos Sci* 28(3):513–527
- Kitous S, Bensalem R, Adolphe L (2012) Airflow patterns within a complex urban topography under hot and dry climate in the Algerian Sahara. *Build Environ* 56:162–175
- Kovar-Panskus A, Moulinneuf L, Savory E, Abdelqari A, Sini JF, Rosant JM, Robins A, Toy N (2002) A wind tunnel investigation of the influence of solar-induced wall-heating on the flow regime within a simulated urban street canyon. *Water Air Soil Pollut Focus* 2:555–571
- Kwak KH, Baik JJ, Lee SH, Ryu YH (2011) Computational fluid dynamics modelling of the diurnal variation of flow in a street canyon. *Boundary-Layer Meteorol* 141(1):77–92
- Lawrence Berkeley Laboratory (LBL) (1994) DOE2.1E-053 source code
- Letzel MO, Krane M, Raasch S (2008) High resolution urban large-eddy simulation studies from street canyon to neighbourhood scale. *Atmos Environ* 42:8770–8784
- Li XX, Britter RE, Norford LK, Koh TY, Entekhabi D (2012) Flow and pollutant transport in urban street canyons of different aspect ratios with ground heating: large-eddy simulation. *Boundary-Layer Meteorol* 142(2):289–304
- Louka P, Vachon G, Sini JF, Mestayer PG, Rosant JM (2002) Thermal effects on the flow in a street canyon—Nantes’99 experimental results and model simulations. *Water Air Soil Pollut Focus* 2:351–364
- Nakamura Y, Oke TR (1988) Wind, temperature and stability conditions in an east-west oriented urban canyon. *Atmos Environ* 22:2691–2700
- Offerle B, Eliasson I, Grimmond CSB, Holmer B (2007) Surface heating in relation to air temperature, wind and turbulence in an urban street canyon. *Boundary-Layer Meteorol* 122:273–292
- Park SB, Baik JJ (2013) A Large-eddy simulation study of thermal effects on turbulence coherent structures in and above a building array. *J Appl Meteorol Climatol* 52(6):1348–1365
- Park SB, Baik JJ, Raasch S, Letzel MO (2012) A large-eddy simulation study of thermal effects on turbulent flow and dispersion in and above a street canyon. *J Appl Meteorol Clim* 51(5):829–841
- Park SB, Baik JJ, Ryu YH (2013) A large-eddy simulation study of bottom-heating effects on scalar dispersion in and above a cubical building array. *J Appl Meteorol Climatol* 52(8):1738–1752

- Pedersen CO, Liesen RJ, Strand RK, Fisher DE, Dong L, Ellis PG (2001) A toolkit for building load calculations; Exterior Heat Balance (CD-ROM). American Society of Heating Refrigerating and Air Conditioning Engineers (ASHRAE). Building Systems Laboratory
- Perret L, Savory E (2013) Large-scale structures over a single street canyon immersed in an urban-type boundary layer. *Boundary-Layer Meteorol* 148(1):111–131
- Raasch S, Schröter M (2001) PALM—a large-eddy simulation model performing on massively parallel computers. *Meteorol Z* 10:363–372
- Richards K, Schatzmann M, Leitl B (2006) Wind tunnel experiments modelling the thermal effects within the vicinity of a single block building with leeward wall heating. *J Wind Eng Ind Aerodyn* 94(8):621–636
- Rosenfeld AH, Akbari H, Bretz S, Fishman BL, Kurn DM, Sailor DJ, Taha H (1995) Mitigation of urban heat islands: materials, utility programs, updates. *Energy Build* 22:255–265
- Shaw RH, Schumann U (1992) Large-eddy simulation of turbulent flow above and within a forest. *Boundary-Layer Meteorol* 61(1–2):47–64
- Sini JF, Anquetin S, Mestayer PG (1996) Pollutant dispersion and thermal effects in urban street canyons. *Atmos Environ* 30:2659–2677
- Solazzo E, Britter RE (2007) Transfer processes in a simulated urban street canyon. *Boundary-Layer Meteorol* 124(1):43–60
- Takimoto H, Sato A, Barlow JF, Moriwaki R, Inagaki A, Onomura S, Kanda M (2011) Particle image velocimetry measurements of turbulent flow within outdoor and indoor urban scale models and flushing motions in urban canopy layers. *Boundary-Layer Meteorol* 140:295–314
- Uehara K, Murakami S, Oikawa S, Wakanatsu S (2000) Wind tunnel experiments on how thermal stratification affects flow in and above urban street canyons. *Atmos Environ* 34:1553–1562
- Vardoulakis S, Fisher BEA, Pericleous K, Gonzalez-Flesca N (2003) Modelling air quality in street canyons: a review. *Atmos Environ* 37:155–182
- Wang ZH, Bou-Zeid E, Smith JA (2012) A coupled energy transport and hydrological model for urban canopies evaluated using a wireless sensor network. *Q J R Meteorol Soc* 139:1643–1657
- Xie X, Huang Z, Wang J, Xie Z (2005) The impact of solar radiation and street layout on pollutant dispersion in street canyon. *Build Environ* 40(2):201–212
- Xie X, Liu CH, Leung DY (2007) Impact of building facades and ground heating on wind flow and pollutant transport in street canyons. *Atmos Environ* 41(39):9030–9049
- Yaghoobian N, Kleissl J (2012a) An indoor-outdoor building energy simulator to study urban modification effects on building energy use—model description and validation. *Energy Build* 54:407–417
- Yaghoobian N, Kleissl J (2012b) Effect of reflective pavements on building energy use. *Urban Clim* 2:25–42
- Yaghoobian N, Kleissl J, Krayenhoff ES (2010) Modeling the thermal effects of artificial turf on the urban environment. *J Appl Meteorol Climatol* 49(3):332–345
- Yazdani M, Klems JH (1994) Measurement of the exterior convective film coefficient for Windows in low-rise buildings. *ASHRAE Trans* 100(1):1087–1096